JOURNAL OF THERMOPHYSICS AND HEAT TRANSFER
Vol. 20, No. 2, April–June 2006

Coupled Radiation, Conduction, and Joule Heating in Argon Thermal Plasmas

Christine Deron,* Philippe Rivière,† Marie-Yvonne Perrin,‡ and Anouar Soufiani§
Centre National de la Recherche Scientifique et École Centrale Paris, 92295 Châtenay-Malabry Cedex, France

A model is developed to study the coupled energy transfer mechanisms and to predict the temperature profiles in axisymmetric atmospheric argon plasmas. The steady-state energy balance equation, including radiation, conduction, and electric heating, is solved iteratively. Radiative transfer is computed from a Monte Carlo method fed by up to date high-resolution spectroscopic data and accurately predicted line profiles. The model is first validated through comparisons with experimental results obtained via emission spectroscopy from a Maecker-type, direct current, wall-stabilized argon plasma. Different techniques were used for the measurement of temperature and electron number density profiles and to assess the local equilibrium character of this plasma. It is shown that radiative losses leads to a significant decrease of the temperature level and that self-absorption inside the plasma column is very important. The contribution of different spectral domains to radiative transfer is analyzed, and a parametric study is conducted by varying the arc current intensity.

Nomenclature

c	=	vacuum light velocity
E	=	electric field
E_{thin}	=	total radiative power emitted by the plasma
e	=	electron charge
h	=	Planck constant
I	=	electric current intensity
I_ν^0	=	Planck function
k_B	=	Boltzmann constant
m_e	=	electron mass
n_e	=	electron density
n_i	=	density of level i of Ar or Ar^+ atom
P_R	=	radiative power per unit volume
$\boldsymbol{q}^{\text{rad}}$	=	radiative flux vector
q_r^{rad}	=	radial component of $\boldsymbol{q}^{\text{rad}}$
R	=	cylinder radius
r	=	radial position
$\boldsymbol{r}$	=	position vector
S_r	=	optically thin radiation source strength
s	=	abscissa along an optical path
T	=	temperature
κ_ν	=	spectral absorption coefficient
λ	=	thermal conductivity
ν	=	wave number
σ	=	electric conductivity

Received 15 April 2005; revision received 8 June 2005; accepted for publication 9 June 2005.

*Ph.D. Student, Laboratoire Énergétique Moléculaire et Macroscopique, Combustion; currently Process Engineer, SNECMA, 171 Boulevard Valmy-BP 31, F-92702 Colombes Cedex, France.

†Research Scientist, Laboratoire Énergétique Moléculaire et Macroscopique, Combustion, Unité Propre de Recherche 288, Grande Voie des Vignes.

‡Senior Scientist, Laboratoire Énergétique Moléculaire et Macroscopique, Combustion, Unité Propre de Recherche 288, Grande Voie des Vignes.

§Senior Scientist, Laboratoire Énergétique Moléculaire et Macroscopique, Combustion, Unité Propre de Recherche 288, Grande Voie des Vignes.

I. Introduction

In many systems involving electrical arcs, such as high-power light sources, electrical circuit breakers, welding devices, or arc furnaces, radiative transfer is a important mechanism that influences the temperature field evolution inside the system. Its prediction remains a difficult task because the optically thin or thick approximations are generally not valid over all of the spectrum and the contribution of many strong lines have to be accounted for. Moreover, the coupling between the radiative transfer and other energy transfer mechanisms (Joule effect, heat conduction, etc.) may be strong inside arc plasmas because of the high-temperature levels and of the strong variations of the plasma radiative properties with temperature. Many authors have studied this coupling using several approximations. Lowke[1] has calculated the temperature profile inside a steady one-dimensional axisymmetric sodium plasma by solving exactly the radiative transfer equation, but only two D lines were considered in this study. Lowke and Capriotti[2] achieved a similar work in the case of air discharges at 30 atm. They only considered continuum radiation and used the P_1 approximation, which was shown to be quite accurate when compared to full radiative transfer calculations for a given temperature profile. Nevertheless, if line radiation is accounted for, more intermediate optical thicknesses are involved, that is, never thin nor thick, and the P_1 approximation should be less accurate. Lowke et al.[3] have used the same approximation to study the decay of arc plasmas after the removal of the electric field. In the case of argon plasmas, they have assumed the arc to be optically thin, which is questionable for current intensities around 100 A as it will be shown later.

More recently, Gogel et al.[4] have calculated the radiative transfer and temperature profiles inside air and ammonia plasma columns by using a Monte Carlo approach to solve the radiative transfer equation. They neglected line contribution in the case of air plasmas and only accounted for a few lines in the ammonia case. Menart et al.[5] and Menart[6] have used a line-by-line high-resolution description of the radiative properties of argon plasmas and a S_N discrete ordinate method to calculate the radiative transfer inside a two-dimensional axisymmetric arc. The required CPU times were too prohibitive to allow the coupling of radiative transfer with the other mechanisms to determine the temperature field.

Some cruder approximations, which avoid solving the radiative transfer equation have been widely used in such coupled problems. The net emission coefficient method[7] allows the calculation of the radiative losses in the high-temperature regions of the plasma by using an adjustable characteristic length but cannot account for absorption in the colder regions. The partial characteristics method overcomes this drawback by using a tabulation of the radiative

exchange between any two points of the plasma, by assuming a linear temperature profile between them.[8,9] This last assumption may be inaccurate in presence of high-temperature gradient regions. This method has been successfully implemented for the prediction of radiative transfer in SF_6 plasmas, for instance.[10,11] Gidalevich et al.[12] have used another simplifying assumption to study high-pressure argon plasma: They adopted the diffusion Rosseland approximation, which is questionable when considered over all of the spectrum.

To our knowledge, there is a need of experimental validation of the predicted temperature fields obtained from coupled calculations with radiation. In the present work, we consider an atmospheric axisymmetric argon plasma in a steady state and study the effects of radiative transfer on the temperature distribution. The energy balance equation of the plasma is solved iteratively including Joule heating, conduction, and radiation. A detailed description of the high-resolution plasma radiative properties, including continuum and line contributions, is adopted, and the radiative transfer equation is solved through a Monte Carlo method. Results of this model are compared to experimental temperature and electron density measurements inside a wall-stabilized plasma. The radiative transfer and its influence on the temperature field is analyzed, and a parametric study vs the current intensity is then conducted. The theoretical and numerical models, especially the spectroscopic data used for modeling the high-resolution argon spectra and the coupling method, are presented in Sec. II. The experimental setup and measurement techniques are described in Sec. III, and the results are given in Sec. IV.

II. Plasma Modeling

We consider a one-dimensional axisymmetric argon plasma in steady state at local thermodynamic and chemical equilibrium. Under these assumptions, the plasma composition only depends on the local temperature and pressure. This composition has been determined from the Saha–Eggert, Guldberg–Waage, electroneutrality, and perfect gas law equations. The involved species are Ar, Ar^+, Ar^{2+}, and Ar^{3+} and electrons; atomic and ion internal partition functions have been computed from National Institute of Standards and Technology (NIST) spectroscopic data[13] (level and ionization energies) completed according to an hydrogenoid model. The lowering of the ionization potentials have been evaluated using the classical Debye–Hückel theory (see Ref. 14). The pressure is assumed uniform and equal to 1.07 atm for comparisons with measurements and the plasma at rest. The electric field E is assumed uniform and parallel to the symmetry axis. The plasma state is, thus, uniquely characterized by the radial temperature field $T(r)$, which will be determined by solving the energy balance equation. The ability of this simple model to describe the experimentally studied plasma will be discussed in Sec. III.

A. Temperature Distribution

The energy balance equation under the preceding hypotheses is

$$\frac{1}{r}\frac{\mathrm{d}}{\mathrm{d}r}\left(r\lambda\frac{\mathrm{d}T}{\mathrm{d}r}\right)-\frac{1}{r}\frac{\mathrm{d}}{\mathrm{d}r}\left(rq_r^{\mathrm{rad}}\right)+\sigma E^2=0 \tag{1}$$

where λ and σ designate the thermal and electric conductivities, respectively, and q_r^{rad} is the radial radiative flux. The temperature-dependent transport coefficients σ and λ have been taken from Ref. 15. The electric field is determined by imposing the value of the current intensity I inside the arc following

$$I=E\int_0^R 2\pi r\sigma\,\mathrm{d}r \tag{2}$$

where R is the arc boundary radius. The divergence of the radiative flux is obtained from the radiative transfer equation according to

$$\frac{1}{r}\frac{\mathrm{d}}{\mathrm{d}r}\left(rq_r^{\mathrm{rad}}\right)=\int_\nu \mathrm{d}\nu\kappa_\nu(\boldsymbol{r})\left\{4\pi I_\nu^0(\boldsymbol{r})-\int_{\boldsymbol{r}'}\kappa_\nu(\boldsymbol{r}')I_\nu^0(\boldsymbol{r}')\right.$$
$$\left.\exp\left[-\int_{s=0}^{\|\boldsymbol{r}'-\boldsymbol{r}\|}\kappa_\nu\left(\boldsymbol{r}+s\frac{\boldsymbol{r}'-\boldsymbol{r}}{\|\boldsymbol{r}'-\boldsymbol{r}\|}\right)\mathrm{d}s\right]\frac{\mathrm{d}\boldsymbol{r}'}{\|\boldsymbol{r}'-\boldsymbol{r}\|^2}\right\} \tag{3}$$

where $\kappa_\nu(\boldsymbol{r})$ is the spectral absorption coefficient of the plasma at location $\boldsymbol{r}$ and wave number ν and $I_\nu^0(\boldsymbol{r})$ is the Planck function at temperature $T(\boldsymbol{r})$. In Eq. (3), the reflection of radiation at the arc boundary walls has been neglected just as the emission from these walls. The wall temperature will be imposed to a low prescribed value around 500 K, which allows the neglect of the boundary emission. We have checked the sensitivity of the calculated temperature profiles to wall reflection. When wall reflection is accounted for with an isotropic reflectivity of 0.2, the maximum increase of the temperature is about 60 K, which remains much smaller than experimental uncertainties discussed in Sec. III. The radiative properties of the plasma (namely, the spectral absorption coefficient κ_ν) have been obtained from a line-by-line procedure and are described in Sec. II.B. Equations (1–3) have been solved in a coupled manner by imposing the current intensity I, the temperature at the arc boundary $T(r=R)=500$ K, and the symmetry condition $\mathrm{d}T/\mathrm{d}r=0$ at $r=0$. The numerical implementation is discussed in Sec. II.C.

B. Argon Radiative Properties

The absorption spectra of the plasma have been calculated from the equilibrium plasma composition at the pressure1.07 atm and in the temperature range 1000–15,000 K by including Ar and Ar^+ lines, the photoionization continuum, and the Bremsstrahlung contribution. The spectral range retained extends from 1000 to 150,000 cm^{-1}.

Ar and Ar^+ line positions and intensities have been taken from the NIST database.[13] Their contribution to the absorption spectra has been included by considering a Voigt profile accounting for Doppler, van der Waals, resonance, and Stark broadening. Van der Waals and resonance broadening linewidths of Ar have been obtained from the classical C_6 and C_3 expressions[14] and the Opacity Project Team database (TOPBASE)[16] in a similar way to that described in Ref. 17 for air plasmas. Stark widths of Ar lines have been evaluated following the semiclassical perturbative impact approach of Sahal-Bréchot for electron contributions.[18,19] The inelastic contribution is limited to the second-order dipolar term, whereas the elastic one only includes the dipolar fourth-order polarization and the quadrupolar second-order terms. Inelastic cross section symmetrization and impact parameter cutoff procedures of Ref. 19 have been used. The ion contribution to the Stark broadening has been included from the quasistatic correction given by Griem.[14] The detailed expressions that have been used may be found in Ref. 20. The oscillator strengths, transition Bohr frequencies, and quantum defects required when evaluating these expressions have been taken from TOPBASE.[16] Comparisons between our calculations and various experimental results available in the literature[21–24] are shown in Fig. 1 for the main Ar lines in the visible spectrum. The typical deviation between our results and experimental values is about 30% except for two lines, namely, the $^2P^*_{1/2}4s\,^2[1/2]_1-{}^2P^*_{3/2}5p\,^2[3/2]_1$ transition near 459.6097 nm and

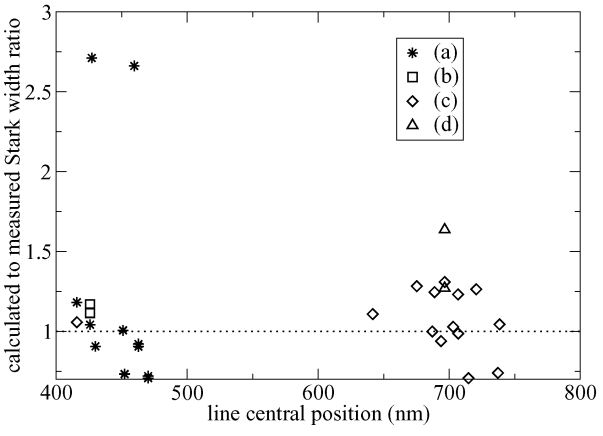

Fig. 1 Ratio of calculated Stark linewidths to measured for various visible Ar lines vs their central wavelength position; calculated values obtained in present study and ∗, Ref. 21; □, Ref. 22; ◇, Ref. 23; and △, Ref. 24.

the $^2P^*_{3/2}4s\,^2[3/2]_1 - {}^2P^*_{3/2}5p\,^2[3/2]_1$ line near 427.2169 nm, for which we observe a factor of about 2.75 between measured and calculated values. These discrepancies may be attributed to an erroneous oscillator strength involving the $3s^2 3p^5 5p^1 P^e$ term in the TOPBASE compilation. Nevertheless, these discrepancies will have no incidence on the radiative transfer because these two lines remain optically thin in our application. In a similar way, Ar^+ lines are optically thin because of the low ionization degree of the plasma in the considered temperature range, and so their contribution has been included by only considering a Doppler profile.

The photoionization continuum of Ar and Ar^+ species has been calculated from the photoionization cross sections $\Sigma_i(\nu)$ given in Ref. 16 for each level i. The resulting absorption coefficient is

$$\kappa_\nu^{bf} = \left[1 - \exp\left(-\frac{hc\nu}{k_B T}\right)\right] \sum_i n_i \Sigma_i(\nu) \tag{4}$$

where n_i is the density of level i.

The electron–ion Bremsstrahlung contribution has been evaluated through the classical Kramers formula (see Ref. 25) corrected by an hydrogenoid Gaunt factor $g(\nu, T)$ (see Ref. 26). The corresponding absorption coefficient is given by

$$\kappa_\nu^{ei} = g(\nu, T)\frac{4}{3}\sqrt{\frac{2\pi}{3k_B T m_e}}\frac{e^6}{m_e h\nu^3 c^4 (4\pi\varepsilon_0)^3} \times \left[1 - \exp\left(-\frac{hc\nu}{k_B T}\right)\right] n_e n_i \tag{5}$$

where n_e designates the electron number density, e and m_e are the electron charge (International System of Units) and mass, respectively, and ϵ_0 is the vacuum dielectric constant. The Gaunt factors have been taken from Ref. 27 for temperatures higher than 12,000 K and from Ref. 28 for lower ones.

The electron–neutral Bremsstrahlung contribution has been evaluated from the electron impact momentum transfer cross sections following Cabannes and Chapelle,[29]

$$\kappa_\nu^{eo} = \frac{16e^2 n_e n_o}{4\pi\epsilon_0 3hc^4\nu^3}\left(\frac{k_B T}{2\pi m_e}\right)^{\frac{3}{2}} Q_1(T)\left[1 - \exp\left(-\frac{hc\nu}{k_B T}\right)\right] \times \left[1 + \left(1 + \frac{hc\nu}{k_B T}\right)^2\right] \tag{6}$$

where n_o designates the Ar atom number density. The momentum transfer cross sections $Q_1(T)$ have been taken from Ref. 15. Comparisons between the results obtained from Eq. (6) and the quantum calculations of Geltman[30] have shown a relative good agreement above 5000 K. (Differences remain in the confidence range of 30% estimated by Deron.[31]) Larger discrepancies have been observed at lower temperatures but have no incidence in our application because the electron–neutral Bremsstrahlung remains optically thin at low temperature and its contribution to the plasma emission is weak.

High-resolution absorption spectra taking into account the earlier described free–free, bound–free and bound–bound contributions have been calculated and stored at temperatures ranging from 1000 to 15,000 K with an incremental step of 1000 K. The spectral resolution used is 0.05 cm^{-1}. Figure 2 shows these plasma absorption spectra at 10,000 and 15,000 K.

Figure 3 shows comparisons between the optically thin source strength of the plasma calculated according to

$$S_r(T) = \int_{\nu_1}^{\nu_2} \kappa_\nu(T) I_\nu^0(T)\,\mathrm{d}\nu \tag{7}$$

from the absorption spectra obtained in the present study and various experimental[32–36] or theoretical[37] results. The spectral range retained when evaluating Eq. (7) extends from 4000 to 40,000 cm^{-1} to be consistent with the experimental results. A quite good agreement is observed between our calculations and the previously published data, providing a partial validation of the radiative properties described earlier.

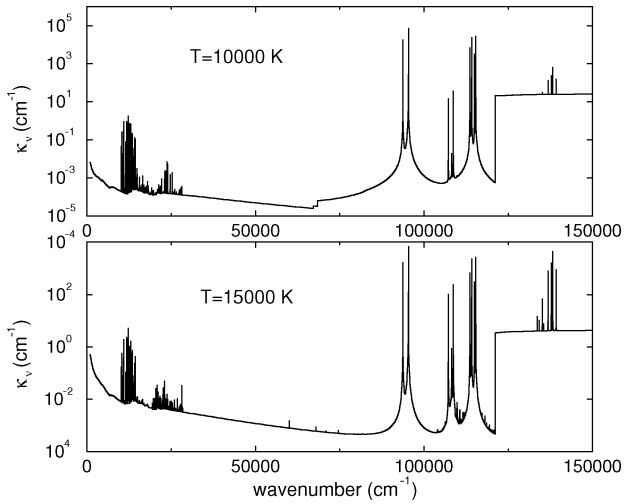

Fig. 2 Predicted argon absorption spectra at 10,000 and 15,000 K under atmospheric pressure.

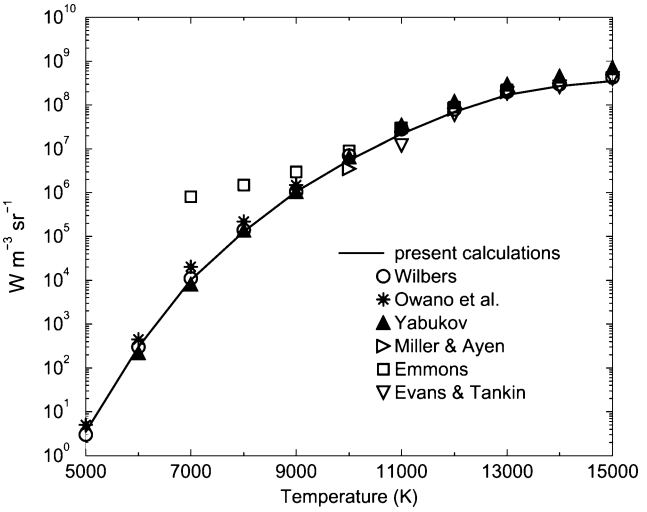

Fig. 3 Optically thin radiative source strength for atmospheric Ar plasma in spectral range 4000–40,000 cm^{-1}; present calculations and results of Owano et al.,[32] Emmons,[33] Evans and Tankin,[35] Miller and Ayen,[34] Wilbers,[36] and Yakubov.[37]

C. Numerical Treatment

Because of the strong and nonobvious dependence of the radiative properties involved in Eq. (3) on the plasma temperature, the coupled solution of Eqs. (1–3) is obtained by using a double iteration between Eqs. (1) and (2) on the one hand and between Eqs. (1) and (2) and Eq. (3) on the other hand. Equations (1) and (2) are solved for a fixed value of the radiative power field, providing a new temperature field. A relaxation factor of typically 0.3 is applied to this new temperature field, and a new radiative power field is then obtained by solving Eq. (3) from this relaxed temperature field. The procedure is iterated until the temperature variations do not exceed 40 K.

In a similar way, the coupled equations (1) and (2) are solved by assuming in a first step that the transport properties σ and λ are fixed to their values obtained from the current temperature field. A new electric field value is then deduced from Eq. (2), and a new temperature field is obtained by inverting the Fourier term in Eq. (1). A classical finite difference discretization on a 1000 points regular grid is used for this inversion. A relaxation factor about 0.01 is applied to this temperature field before evaluating new values of the transport properties and iterating the procedure. The iteration is stopped as soon as the relative variations of the temperature field did not exceed 10^{-6}.

The radiative transfer equation (3) is solved using a Monte Carlo method similar to that described in Ref. 4. In a first step, the total radiative power E_{thin} emitted by the plasma is calculated according to

$$E_{\text{thin}} = \int_0^R 2\pi r \int_{\nu=0}^{\infty} \kappa_\nu(r) I_\nu^0(r)\, \mathrm{d}\nu\, \mathrm{d}r \tag{8}$$

Each of the N energy bundles used during the Monte Carlo run is characterized by the same energy E_{thin}/N. We use then five independent random numbers uniformly distributed between 0 and 1, U_r, U_ν, U_θ, U_φ, and U_ℓ to define the emission point r, the wavenumber ν, the propagation direction $\boldsymbol{u}$ (characterized by the zenithal and azimuthal angles θ and φ), and the absorption length ℓ associated to each bundle respectively, by inverting the following implicit relations:

$$\frac{1}{E_{\text{thin}}} \int_0^r 2\pi r' \int_{\nu=0}^{\infty} \kappa_\nu(r') I_\nu^0(r')\, \mathrm{d}\nu\, \mathrm{d}r' = U_r \tag{9}$$

$$\int_{\nu'=0}^{\nu} \kappa_{\nu'}(r) I_{\nu'}^0(r)\, \mathrm{d}\nu' \Big/ \int_{\nu'=0}^{\infty} \kappa_{\nu'}(r) I_{\nu'}^0(r)\, \mathrm{d}\nu' = U_\nu \tag{10}$$

$$\cos\theta = 1 - 2U_\theta \tag{11}$$

$$\varphi = 2\pi U_\varphi \tag{12}$$

$$\int_{s=0}^{\ell} \kappa_\nu(\boldsymbol{r} + s\boldsymbol{u})\, \mathrm{d}s = -\ell_n U_\ell \tag{13}$$

The radiative power inside each cell of the plasma i, delimited by two cylinders of radius r_i and r_{i+1}, is, thus, obtained from the numbers of emitted N_{ei} and absorbed N_{ai} bundles by the cell i according to

$$\int_{r_i}^{r_{i+1}} 2\pi r \boldsymbol{\nabla}\cdot\boldsymbol{q}^{\text{rad}}\, \mathrm{d}r = \frac{E_{\text{thin}}}{N}(N_{ei} - N_{ai}) \tag{14}$$

Note that the inversion of Eq. (10) is performed using the high-resolution absorption spectrum at point r. The absorption distribution function defined by the left hand side of Eq. (10) is stored for each radial discretization point. To reduce the CPU time required by this inversion, the function $\nu(U_\nu)$ is tabulated beforehand for nine values, $0.1, \ldots, 0.9$, of U_ν at each radial discretization point. This allows the speedup of the search of the wave number corresponding to a given value U_ν by first positioning this value among the nine prescribed ones.

To estimate the variance $\Sigma^2(r)$ of the calculated radiative power $P_R(r) = \boldsymbol{\nabla}\cdot\boldsymbol{q}^{\text{rad}}(r)$, the N energy bundles are grouped in K subsamples of 1,200,000 bundles. Each of these subsamples gives a partial estimation of the radiative power field $P_R^k(r)$, $k = 1, \ldots, K$; the radiative power is estimated according to

$$P_R(r) = \sum_k P_R^k(r)$$

and its variance according to

$$\Sigma^2(r) = \frac{1}{K(K-1)} \sum_{k=1}^{K} \left[P_R^k(r) - P_R(r)\right]^2 \tag{15}$$

Figure 4 shows the standard deviation estimations in the case of the temperature profile obtained for a current intensity of 100 A and an arc radius of 2.5 mm and for different values of N. We may observe the classical convergence of the Monte Carlo method in $N^{-1/2}$. The standard deviation remains lower than 2% of the radiative power as soon as K is higher than 300 except at the center of the arc where the convergence is slower: Very few bundles are emitted or absorbed by cells near the arc center because of their small area. This lack of convergence has no influence on the predicted temperature profile because the radiative source term, integrated over the central cell, tends to zero.

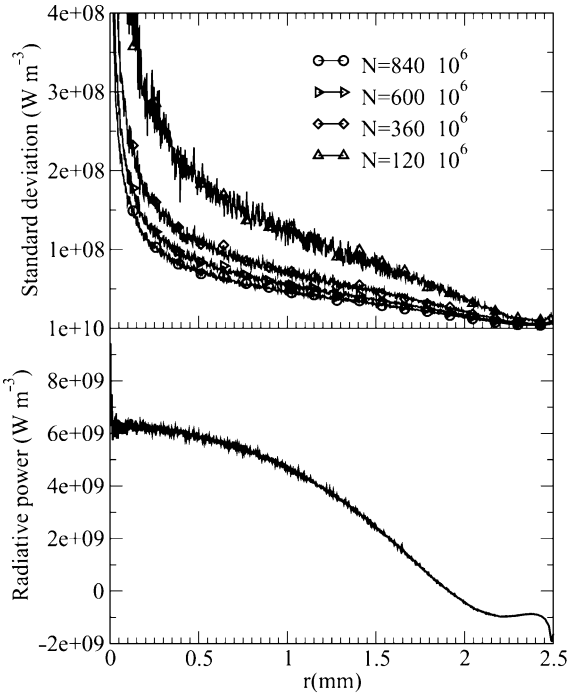

Fig. 4 Standard deviation (top) of radiative power field (bottom) calculated by Monte Carlo method for various bundle numbers N; temperature field corresponds to current intensity of 100 A (see Fig. 13).

III. Experimental Setup and Measurement Techniques

A Maecker-type wall stabilized arc is used to produce a direct current stable argon plasma at atmospheric pressure. Detailed descriptions of this plasma source and of temperature and electron number density measurement techniques are provided in Refs. 31 and 38. We briefly recall here the main characteristics of this device and the measurement techniques based on emission spectroscopy.

Figure 5 shows the experimental setup including the Maecker chamber and the optical components. The chamber is made of 12 electrically insulated, 5.5-mm-thick copper plates with a 5 mm inner diameter where the dc discharge takes place along 75 mm total length. The length to diameter ratio is equal to 15, which is sufficiently high to allow one-dimensional cylindrical modeling of radiative transfer in the central part of the arc column. Four anodes and four cathodes, made of thoriated tungsten, are used to ensure an axisymmetric plasma column. The discharge is initiated at low pressure (typically 200 Pa) and high voltage (typically 1 kV), and then a lower voltage is applied and the pressure is increased to the desired value. The plasma source can be operated in steady conditions between 40 and 150 A under a maximum voltage of 200 V. The electrodes and copper plates are cooled with a circuit of deionized water. Quartz windows allow optical investigations of the plasma column either axially or radially.

The radial plasma emission spectra were measured in the spectral range 400–1000 nm. A 1340×400 pixel charge-coupled-device camera, placed at the exit of a 500-mm focal length spectrometer, is optically conjugated to the plasma diameter at the middle of the 75-mm-long plasma column through an achromatic doublet of 200-mm focal length. The spectra were recorded with a typical spectral resolution of 0.03 nm and calibrated with a 45 W quartz-tungsten-halogen (QTH) lamp. Only relative calibration was carried out because it was not possible to introduce the QTH lamp inside the plasma chamber.

The spectra were first Abel inverted to produce local emission coefficients in optically thin spectral regions. Several techniques were then applied to extract electron densities $n_e(r)$ and temperature radial profiles. For electron concentration, the argon flow (typically 44.4 cm$^3 \cdot$ s^{-1}) was seeded with hydrogen (0.11 cm$^3 \cdot$ s^{-1}) and $n_e(r)$ was deduced from the adjustment of H_α and H_β line profiles. For these lines, the measured profiles were adjusted to fit Voigt profiles

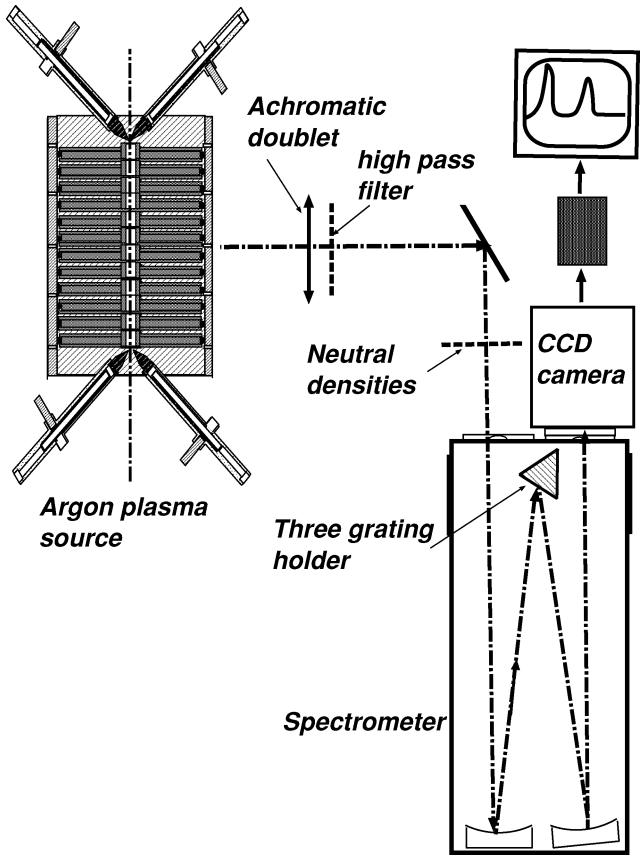

Fig. 5 Plasma chamber and optical setup arrangement.

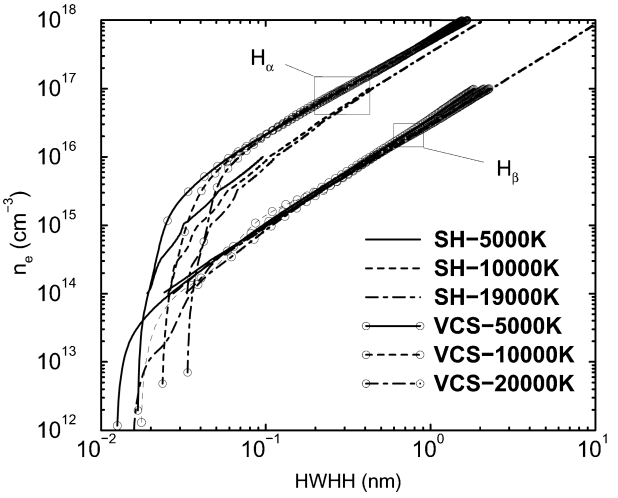

Fig. 6 Comparison between electron number densities deduced from tabulations of Ref. 39 (SH) and of Ref. 40 (VCS) for H_α and H_β line profiles at various temperatures.

using the tabulated collisional shapes of Ref. 39 (tabulated online at http://cdsweb.u-strasbg.fr/htbin/cat?VI/98 [cited 14 July 2000]). These data were found more reliable than those of Ref. 40. Figure 6 shows comparisons between electron number densities deduced from the microfield method of Ref. 39 and those from the unified theory of Vidal et al.[40] as functions of line half-widths at half-height and temperature. A good agreement is obtained for the H_β line, but a factor as high as two is observed for the H_α line. The data of Ref. 39 are preferred in this study because they provide consistent measurements from both H_α and H_β lines, which is not the case for the data of Ref. 40. Figure 6 shows also that the temperature dependence of hydrogen line half-widths is very weak for electron densities higher than 5×10^{15} cm^{-3} for H_α and than 10^{14} cm^{-3} for H_β line. In practice, this temperature dependence has been accounted for by using the temperature profile measured from Ar^+ lines (described later) in the adjustment of line profiles. Apart from the accuracy of the theoretical hydrogen line profiles, the uncertainties of electron number densities result from the experimental uncertainty on line profile determination (mainly the linewidth) and, to a lesser extent, from the uncertainty on local temperature measurement. An estimation of linewidth measurement uncertainty of about 10% leads to an uncertainty on n_e of 14%. On the other hand, above $n_e = 5 \times 10^{15}$ cm^{-3}, an uncertainty of about 500 K on the temperature induces an uncertainty of 5% on n_e when deduced from the H_α line profile.

Three different techniques were used for the determination of temperature profiles and for the assessment of local thermal equilibrium in the plasma. The first one uses Boltzmann plots of Ar^+ line intensities vs the energy of the upper level of the considered transition. Four Ar^+ lines (442.600, 460.957, 473.591, and 480.602 nm) were selected on the basis of their isolated positions and their suitable optical thickness. The uncertainties associated with the Boltzmann plots of Ar lines (404.442, 415.859, 430.010, 696.543, 714.704, and 935.422 nm) were found too high, and the measurement was very sensitive to the precise calibration of the emission spectra over a very wide spectral range. The second method uses the ratio between the intensities of closely located Ar and Ar^+ lines. Assuming a Saha–Eggert equilibrium, the ratio of the intensities of these transitions provides a sensitive temperature measurement if the electron number density is known (see Ref. 14). We use the $n_e(r)$ measurements already described and the Ar line at 430.010 nm in association with the several Ar^+ lines listed earlier. In the third technique, the plasma is assumed to be singly ionized (with Ar^{++} neglected) and the temperature is deduced from the ratio between the intensity of the Ar line at 430.010 nm and the adjacent radiative recombination continuum (at 410 nm). Here also, a partial equilibrium is assumed and we use Hofsaess photoionization cross sections.[41] The data from Hofsaess are in very good agreement in this spectral region with many experimental or other theoretical data (for instance, Ref. 42).

Figure 7 shows a portion of a typical experimental spectrum with Ar and Ar^+ lines used for temperature measurements. An estimation of temperature uncertainties was carried out for each of the three techniques. When it is assumed that the uncertainties on measured line intensities are about 10%, and the uncertainties on line strengths (taken from the NIST atomic database) and electron number densities are neglected, the uncertainties on the measured temperature around 14,000 K are 820, 156, and 640 K when using the Boltzmann method with Ar^+ lines, Ar^+ to Ar line intensity ratio, and Ar line to continuum ratio, respectively. The ratio between Ar^+ and Ar line intensities provides obviously the highest sensitivity because the energy difference involved in the method is about

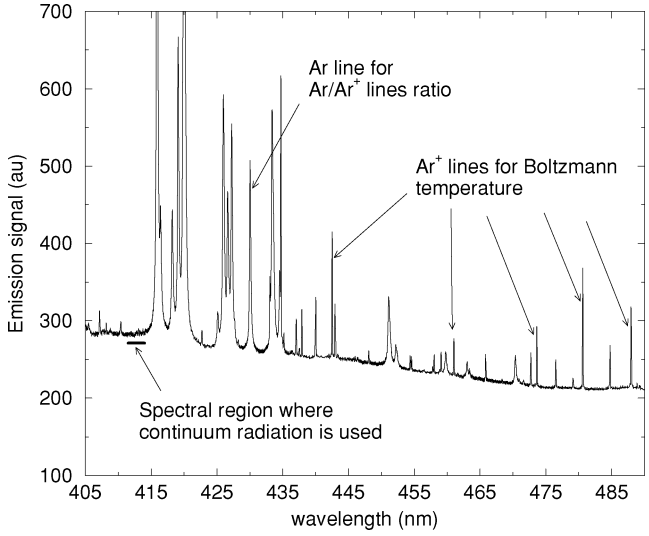

Fig. 7 Portion of an experimental spectrum showing Ar and Ar^+ lines and continuum radiation used for temperature measurements.

165,000 cm^{-1}, whereas the other methods involve energy differences of about 15,500 cm^{-1} for the first method and 14,800 cm^{-1} for the third method. The use of Ar^+ to Ar line intensities relies, however, on the local thermodynamic equilibrium (LTE) assumption. If we include an uncertainty of about 15% on n_e, the uncertainty on the temperature deduced from the ratio between Ar^+ and Ar line intensities becomes close to 460 K.

IV. Results and Discussion

In this section, we first compare experimental results with predictions in the experimental conditions and then present a parametric study for various values of the current. The experimental conditions considered correspond to a current $I = 101 \pm 0.1$ A and a total argon flow rate equal to 44.44 $cm^3 \cdot s^{-1}$. Argon was seeded with a 0.11 $cm^3 \cdot s^{-1}$ flow of hydrogen, and the total pressure was fixed to 1.07 atm. Simple estimation of the convective heat flux, based on the measured Ar flow rate and on an outlet temperature of about 10,000 K, shows that the convective flux is limited to about 4% of the injected electric power. The contribution of convection in the energy balance can then be neglected because, if the electric power is increased, for instance, by 10%, the maximum plasma temperature is only increased by about 75 K, which remains small in comparison with experimental uncertainties. A discussion on the contribution of convective terms in cascaded arc plasmas may be found in Ref. 43.

Figure 8 shows a comparison of the temperature profiles deduced from the three experimental techniques. For the second technique (Ar^+ to Ar line intensity ratio), the temperature shown corresponds to an averaged temperature obtained from the five Ar^+ lines shown in Fig. 7 in association with the Ar line centered at 430.010 nm. The electron number density is the density measured from the H_α line presented later. The dispersion of the results from the five Ar^+ line measurements remains limited to 200 K. The differences between the results from the three techniques are within the estimated experimental uncertainties discussed earlier. This tends to prove that the assumption of thermal equilibrium is reasonable for this atmospheric plasma, at least for $r < 2$ mm. Another issue concerning the comparison between different methods for temperature determination is their ability to cover a wide temperature range. Chemical composition calculations under equilibrium show that Ar^+ concentration decreases strongly with temperature below, typically, 10,000 K. The use of Ar^+ lines becomes impractical below this temperature because the emission signal is too weak. Thus, the measurements from Ar lines and continuum cover a wider spatial range in Fig. 8.

Comparisons between measured and calculated temperature profiles under various assumptions concerning radiative transfer are also shown in Fig. 8. A good agreement between calculated and measured temperature profiles is observed, especially in the central part of the plasma column. Differences up to 800 K are observed in the intermediate region $1 < r < 2$ mm. These differences could be the result of experimental uncertainties slightly higher than the estimated ones, a nonuniform electric field, or a local effect of the flowfield, although the global convective loss is estimated to less

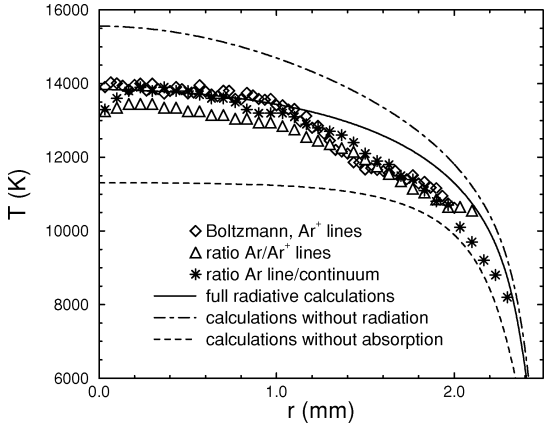

Fig. 8 Comparison between measured and computed temperature profiles.

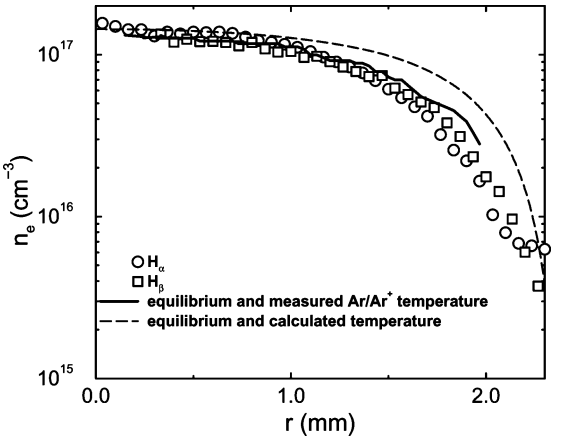

Fig. 9 Electron number densities from H_α and H_β lines and from equilibrium composition and measured or calculated temperature profiles.

than 4% of the total electric power. Note that calculations without radiation overestimate the maximum temperature by about 1600 K. On the other hand, calculations taking into account emission, but not absorption, underestimate the maximum temperature by about 2700 K. This shows that the medium cannot be considered as optically thin and that most of the emitted radiation is trapped inside the plasma column, which increases the temperature level.

The measured electron number densities are shown on Fig. 9. We can notice first that there is a remarkable agreement between the densities deduced from H_α and H_β lines. This agreement shows the reliability of the theoretical data of Stehlé and Hutcheon[39] on which the measurements are based. Figure 9 also shows a comparison of the experimental electron densities with the densities deduced from equilibrium composition calculations combined with the temperatures deduced from the ratio between Ar^+ and Ar line intensities. The observed good agreement also confirms the local thermodynamic and chemical equilibrium character of this plasma. The electron number densities deduced from the calculated temperature profile and chemical composition at equilibrium are slightly higher than the measured ones in the region $1 < r < 2$ mm. This is a result of the slight overestimation of the calculated temperatures in this region.

As a global validation of the theoretical model developed here, we have compared the measured emission spectra with calculated ones. The latter have been computed from the experimental temperature profile (ratio between Ar^+ and Ar line intensities) and by integrating the radiative transfer equation on a line of sight of the plasma, as in the experiment. Figure 10 shows an example of comparisons for a line of sight 0.33 mm away from the plasma axis. The absolute calibration of the experimental spectrum shown in Fig. 10 was carried out by first adjusting it to the theoretical one at 410 nm. Comparisons between local experimental continuum emission and the results from Ref. 42 revealed a defect in our relative calibration with the QTH lamp for wavelengths higher than 650 nm. A second calibration coefficient (varying linearly between 1 at 650 nm and 1.65 at 850 nm) was, thus, determined from line-free spectral regions and applied to the experimental spectrum. Recall that temperatures and electron densities are measured here from emission in the spectral range limited to 410–485 nm and are not concerned with this lack of accurate calibration over the whole spectrum. This fact also led us to not consider temperature measurements from Boltzmann plots of argon lines, which required the use of lines in the red or the near-infrared region. Figure 10 shows that the overall agreement between predicted and calculated spectra is good. Detailed comparisons (see Ref. 31) show, however, that the measured continuum in the range 450–550 nm and above 750 nm is slightly higher than the predicted one. This could be attributed, on the one hand, to the lack of photoionization cross sections from high-energy levels in the TOPBASE data and, on the other hand; to the lack of a precise calibration of our experimental setup over the whole spectral region.

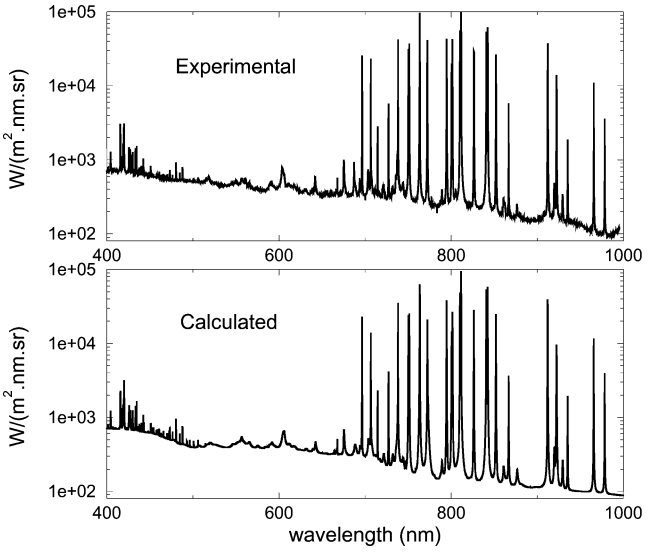

Fig. 10 Experimental and calculated emission intensities from plasma path at 0.33 mm above center.

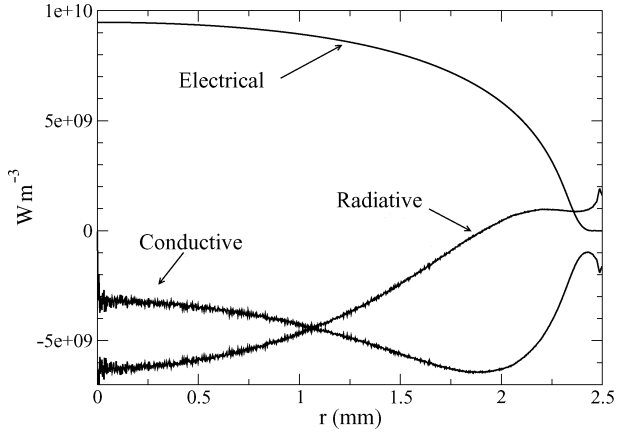

Fig. 11 Computed three terms, σE^2, $1/r$ (d/dr) [$r\lambda$ (dT/dr)], and $-\nabla.q_r$, of energy balance equation.

Table 1 Four regions for spectral analysis of radiative transfer

ν_{min}, cm^{-1}	ν_{max}, cm^{-1}	Name in Fig. 12
10,000	15,000	Lines (visible)
87,000	121,000	Lines (VUV)
121,000	150,000	Continuum (VUV)
1,000	10,000	Continuum (other)
15,000	87,000	Continuum (other)

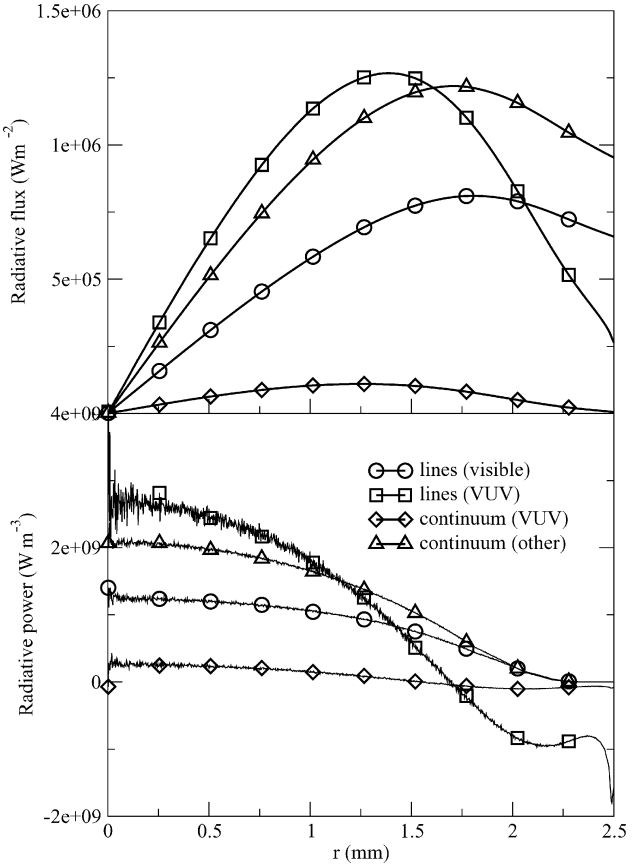

Fig. 12 Spectral contributions to radiative fluxes (top) and radiative powers (bottom); spectral regions defined in Table 1, $I = 101$ A, $R = 2.5$ mm.

For line spectra, the detailed comparisons showed a good agreement concerning both line strengths and linewidths, over all of the considered spectral range from 400 to 1000 nm. A strong self-absorption was found for several Ar lines, and the agreement between measured and calculated profiles of these strong lines is good. We can conclude from these comparisons that both measurements and calculations are reliable because the calculated spectra were based on measured temperature profiles and on the integration of radiative transfer equation.

The different terms of the energy balance equation (1), computed in the experimental conditions described earlier, are compared in Fig. 11. It is shown that the radiative transfer is higher than the conductive one in the central part of the plasma. The radiation source term becomes positive for $r > 2$ mm, which emphasizes the strong absorption by the colder regions of the plasma. Near the wall, the electric source term becomes negligible due to the very small electric conductivity of the medium and low temperature and there is an exact balance between conductive and radiative transfers.

To investigate the spectral contributions to radiative transfer, the spectrum was divided into four regions shown in Table 1, and the contribution of each region to radiative fluxes and radiative powers was determined separately. Figure 12 shows that 1) the contribution of vacuum UV (VUV) continuum radiation is very small; 2) the VUV lines are strongly self-absorbed and their contribution to the radiative flux at the wall is limited to about 13%, although their contribution to pure emission is preponderant; 3) the visible lines (corresponding mainly to transitions between $4s$ and $4p$ states) are slightly self-absorbed and contribute to 36% of the wall radiative flux; and 4) the main contribution is due to the continuum radiation in the UV, visible and infrared ranges [including some weak transitions between $4s$ and $5p$ states, (Fig. 2)]. The lower part of Fig. 12 shows also that the numerical convergence of radiative powers with the Monte Carlo method is less easy in the optically thick spectral regions.

After the detailed analysis of radiative transfer in the described experimental conditions, we have conducted a parametric numerical study where the current intensity is varied and the plasma diameter is kept equal to 5 mm. Figure 13 shows the temperature profiles obtained from the full coupled transfer calculations and when radiation is completely ignored, for a current varying between 50 and 150 A. As expected, the lowering of temperature level, due to radiative losses, increases with the current intensity and reaches about 3800 K for $I = 150$ A. The shape of the temperature profile is also modified for high-current values. Radiative transfer tends indeed to homogenize the temperature profile in the central region as a result of volume to volume exchanges.

Conductive and radiative fluxes at the wall are summarized in Table 2, where are also given the conductive flux computed without radiation and the radiative flux computed without absorption. Although the optically thin emission is very important in comparison with wall conductive fluxes, radiative fluxes remain limited to 18

Table 2 Conductive (q_{cd}) and radiative (q_r) fluxes at the wall

I, A	q_{cd}, MW · m^{-2}	q_r, MW · m^{-2}	$q_{cd,\,\mathrm{wr}}$[a] MW · m^{-2}	$q_{r,\,em}$[b] MW · m^{-2}
50	2.54	0.54	2.76	13.04
75	4.08	1.08	4.53	24.12
100	5.79	1.88	6.59	37.01
125	7.70	2.87	8.89	48.50
150	9.95	3.72	11.39	59.30

[a]Conductive flux obtained without radiation.
[b]Radiative flux if the plasma column is considered as optically thin (no absorption).

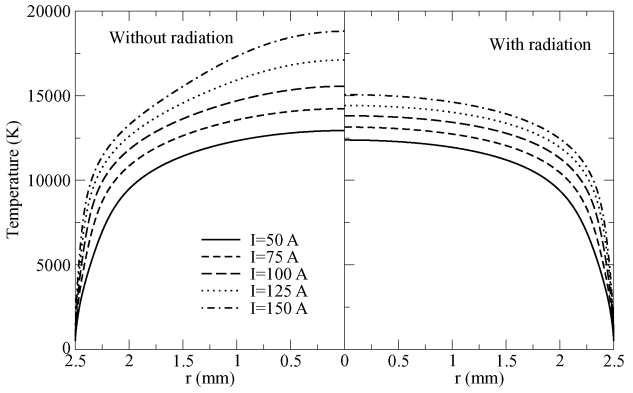

Fig. 13 Temperature profiles computed with and without radiation for various current intensities.

and 27% of the total wall flux for $I = 50$ A and $I = 150$ A, respectively. The total wall flux ($q_{cd} + q_r$) is always slightly higher than the conductive flux computed without radiation.

V. Conclusions

A model for the prediction and analysis of radiative transfer in cylindrical Ar plasma columns was developed. In this model, the energy balance equation, including Joule heating, conduction, and radiation, but neglecting convection, is solved by an iterative method. Radiative transfer is calculated from a high spectral resolution Monte Carlo method, based on up to date spectroscopic data and accurate line shapes.

The model was first validated through comparisons with experimental temperature and electron density measurements in a Maecker-type plasma source and then is used to analyze the spectral behavior of radiative transfer and to conduct a parametric study where the current intensity was varied.

The comparison between various techniques of temperature measurements showed first that the LTE assumption is reasonable in our experimental conditions, at least in the central part of the plasma column. A satisfactory quantitative agreement between predicted and measured temperature profiles and electron number densities was obtained. For a current intensity about 100 A, neglecting radiative transfer leads to an overestimation of the maximum temperature of about 1600 K. On the other hand, the results from the optically thin approximation lead to a strong overestimation of radiative losses and a maximum temperature underestimated by about 2700 K. The spectral analysis of radiative transfer showed a preponderant contribution of the continuum radiation in the visible and UV ranges, and of visible lines, to the escaping radiation. The strong emission of VUV lines and photoionization continuum is mainly self-absorbed and the temperature profile in the central part of the plasma column is flattened for high values of the current intensity, as a result of volume to volume radiative transfer. The total radiative losses of the plasma column vary between 18 and 27% of the total wall flux when the current intensity is varied between 50 and 150 A.

In the present study, a high spectral resolution approach was adopted at the cost of important computational times. Simplified approaches of radiative properties, such as those developed for infrared radiation at lower temperatures are highly desirable for extensive calculations required in unsteady problems, for instance. The development of such approximate models will be the subject of further studies. The results of the present study can be used as a reference for model benchmarking.

Acknowledgment

Computational facilities were made available by the Institut de Développement et des Ressources Informatiques, the Centre National de la Recherche Scientifique computer center in Orsay, France.

References

[1]Lowke, J. J., "A Relaxation Method of Calculating Arc Temperature Profiles Applied to Discharges in Sodium Vapor," *Journal of Quantitative Spectroscopy and Radiative Transfer*, Vol. 9, No. 6, 1969, pp. 839–854.

[2]Lowke, J. J., and Capriotti, E. R., "Calculation of Temperature Profiles of High Pressure Electric Arcs Using the Diffusion Approximation for Radiation Transfer," *Journal of Quantitative Spectroscopy and Radiative Transfer*, Vol. 9, No. 2, 1969, pp. 207–236.

[3]Lowke, J. J., Voshall, R. E., and Ludwig, H. C., "Decay of Electrical Conductance and Temperature of Arc Plasmas," *Journal of Applied Physics*, Vol. 44, No. 8, 1973, pp. 3513–3523.

[4]Gogel, T. H., Sedghinasab, A., and Keefer, D. R., "Radiation Transfer Computation in Cylindrical Arc Columns Using a Monte Carlo Method," *Journal of Quantitative Spectroscopy and Radiative Transfer*, Vol. 52, No. 2, 1994, pp. 179–194.

[5]Menart, J., Heberlein, J., and Pfender, E., "Theoretical Radiative Transport Results for a Free-Burning Arc Using a Line-by-Line Technique," *Journal of Physics D: Applied Physics*, Vol. 32, No. 1, 1999, pp. 55–63.

[6]Menart, J., "Radiative Transport in a Two-Dimensional Axisymmetric Thermal Plasma Using the S-N Discrete Ordinates Method on a Line-by-Line Basis," *Journal of Quantitative Spectroscopy and Radiative Transfer*, Vol. 67, No. 4, 2000, pp. 273–291.

[7]Lowke, J. J., "Predictions of Arc Temperature Using Approximate Emission Coefficients for Radiation Losses," *Journal of Quantitative Spectroscopy and Radiative Transfer*, Vol. 14, No. 2, 1974, pp. 111–122.

[8]Sevast'yanenko, V. G., "Radiation Transfer in a Real Spectrum. Integration over frequency," *Journal of Engineering Physics*, Vol. 36, No. 2, 1979, pp. 138–148.

[9]Sevast'yanenko, V. G., "Radiation Transfer in a Real Spectrum. Integration with Respect to the Frequency and Angles," *Journal of Engineering Physics*, Vol. 38, No. 2, 1980, pp. 173–179.

[10]Aubrecht, V., and Lowke, J. J., "Calculations of Radiation Transfer in SF_6 Plasmas Using the Method of Partial Characteristics," *Journal of Physics D: Applied Physics*, Vol. 27, No. 10, 1994, pp. 2066–2073.

[11]Raynal, G., and Gleizes, A., "Radiative Transfer Calculation in SF_6 Arc Plasmas Using Partial Characteristics," *Plasma Sources Science and Technology*, Vol. 4, No. 1, 1995, pp. 152–160.

[12]Gidalevich, E., Goldsmith, S., and Boxman, R. L., "Theoretical Modelling of High Pressure Argon Arc Radiation," *Plasma Sources Science Technology*, Vol. 11, No. 4, 2002, pp. 513–519.

[13]Martin, W. C., Fuhr, J. R., Kelleher, D. E., Musgrove, A., Sugar, J., Wiese, W. L., Mohr, P. J., and Olsen, K., "NIST Atomic Spectra Database (version 2.0)," [online database], URL: http://physics.nist.gov/asd2 [cited 31 March 2005].

[14]Griem, H. R., *Principles of Plasma Spectroscopy*, Cambridge Univ. Press, 1997.

[15]Devoto, R. S., "Transport Coefficients of Ionized Argon," *Physics of Fluids*, Vol. 16, No. 5, 1973, pp. 616–623.

[16]Opacity Project Team, *The Opacity Project*, Vol. 1, Inst. of Physics Publ., Bristol, England, U.K., 1995.

[17]Chauveau, S., Deron, C., Perrin, M.-Y., Rivière, P., and Soufiani, A., "Radiative Transfer in LTE Air Plasmas for Temperatures up to 15000 K," *Journal of Quantitative Spectroscopy and Radiative Transfer*, Vol. 77, No. 2, 2003, pp. 113–130.

[18]Sahal-Bréchot, S., "Théorie de l'élargissement et du déplacement des raies spectrales sous l'effet des chocs avec les électrons et les ions dans l'approximation des impacts," *Astronomy and Astrophysics*, Vol. 2, No. 3, 1969, pp. 322–354.

[19]Sahal-Bréchot, S., "Théorie de l'élargissement et du déplacement des raies spectrales sous l'effet des chocs avec les électrons et les ions dans l'approximation des impacts," *Astronomy and Astrophysics*, Vol. 1, No. 1, 1969, pp. 91–123.

[20]Rivière, P., "Systematic Semi-Classical Calculations of Stark Broadening Parameters of NI, OI, NII, OII Multiplets for Modelling the Radiative Transfer in Atmospheric Air Mixture Plasmas," *Journal of Quantitative Spectroscopy and Radiative Transfer*, Vol. 73, No. 1, 2002, pp. 91–110.

[21]Jones, D. W., Wiese, W. L., and Woltz, L. A., "Ion Broadening of Ar I Lines in a Plasma," *Physical Review A: General Physics*, Vol. 34, No. 1, 1986, pp. 450–456.

[22]Djurović, S., Mijatović, R., Kobilarov, R., and Konjević, N., "Stark Width and Shift Temperature Dependence of the Ar I 425.9 nm Line," *Journal of Quantitative Spectroscopy and Radiative Transfer*, Vol. 57, No. 5, 1997, pp. 695–701.

[23]Aparicio, J. A., Pérez, C., del Val, J. A., Gigosos, M. A., de la Rosa, M. I., and Mar, S., "Measurment of Stark Broadening and Shift Parameters of Several Ar I Lines," *Journal of Physics B: Atomic and Molecular Physics*, Vol. 31, No. 22, 1998, pp. 4909–4918.

[24]Vitel, Y., and Skowronek, M., "Noble Gas Line Profiles in Dense Plasmas: I. Argon," *Journal of Physics B: Atomic and Molecular Physics*, Vol. 20, No. 24, 1987, pp. 6477–6491.

[25]Zel'dovich, Y. B., and Raiser, Y. P., *Physics of Shock Waves and High-Temperature Hydrodynamic Phenomena*, Vol. 1. Academic Press, New York, 1966, p. 259.

[26]Karzas, W., and Latter, R., "Electron Radiative Transitions in a Coulomb Field," *Astrophysical Journal Supplements Series*, Vol. 6, May 1961, pp. 167–212.

[27]Stallcop, J. R., and Billman, K. W., "Analytical Formulae for the Inverse Bremsstrahlung Absorption Coefficient," *Plasma Physics*, Vol. 16, No. 12, 1974, pp. 1187–1189.

[28]Menzel, D. H., and Pekeris, C. L., "Absorption Coefficients and Hydrogen Line Intensities," *Monthly Notices of the Royal Astronomical Society*, Vol. 96, No. 1, 1935, pp. 77–111.

[29]Cabannes, F., and Chapelle, J., "Reactions Under Plasma Conditions," *Spectroscopic Plasma Diagnostics*, Vol. 1, Wiley, New York, 1971, Chap. 7.

[30]Geltman, S., "Free-Free Radiation in Electron-Neutral Atom Collisions," *Journal of Quantitative Spectroscopy and Radiative Transfer*, Vol. 13, No. 7, 1973, pp. 601–613.

[31]Deron, C., "Rayonnement thermique des plasmas d'air et d'argon: Modélisation des propriétés radiative et étude expérimentale," Thèse de Doctorat, Ecole Centrale Paris, France, June 2003.

[32]Owano, T. G., Gordon, M. H., and Kruger, C. H., "Measurements of the Radiation Source Strength in Argon at Temperatures Between 5000 and 10 000 K," *Physics of Fluids B*, Vol. 2, No. 12, 1990, pp. 3184–3190.

[33]Emmons, H. W., "Arc Measurement of High-Temperature Gas Transport Properties," *Physics of Fluids*, Vol. 10, No. 10, 1967, pp. 1125–1136.

[34]Miller, R. C., and Ayen, R. J., "Temperature Profiles and Energy Balances for an Inductively Coupled Plasma Torch," *Journal of Applied Physics*, Vol. 40, No. 13, 1969, pp. 5260–5273.

[35]Evans, D. L., and Tankin, R. S., "Measurement of Emission and Absorption of Radiation by an Argon Plasma," *Physics of Fluids*, Vol. 10, No. 6, 1967, pp. 1137–1144.

[36]Wilbers, A. T. M., "A Wall-Stabilized Arc as Light Source for Spectroscopic Technique," Ph.D. Dissertation, Technische Univ. Eindhoven, Eindhoven, The Netherlands, 1991.

[37]Yakubov, I. T., "Energy Emitted by Argon Plasma in Spectral Lines," *Optics Spectroscopy*, Vol. 19, 1965, pp. 277–279.

[38]Deron, C., Perrin, M.-Y., and Soufiani, A., "Comparison Between Various Techniques of Temperature and Electron Number Density Measurements from Emission Spectroscopy in Atmospheric Argon Plasmas," *Proceedings of 6th World Conference on Experimental Heat Transfer, Fluid Dynamics, and Thermodynamics*, Paper 6-b-6, edited by N. Kasagi, S. Muruyama, H. Yoshida, and T. Inoue, Heat Transfer Society of Japan, Tohoku, Japan, 2005.

[39]Stehlé, C., and Hutcheon, R., "Extensive Tabulation of Stark Broadened Hydrogen Line Profiles," *Astronomy and Astrophysics Supplement Series*, Vol. 140, No. 1, 1999, pp. 93–97.

[40]Vidal, C. R., Cooper, J., and Smith, E. W., "Hydrogen Stark Broadening Tables," *Astrophysical Journal Supplement Series*, Vol. 5, Jan. 1973, pp. 37–136.

[41]Hofsaess, D., "Photoionization Cross Sections Calculated by the Scaled Thomas–Fermi Method ($h\nu < 50$ ev)," *Atomic Data and Nuclear Data Tables*, Vol. 24, 1979, pp. 285–321.

[42]D'Yachkov, L., Kurilenkov, Y., and Vitel, Y., "Radiative Continua of Noble Gas Plasmas," *Journal of Quantitative Spectroscopy and Radiative Transfer*, Vol. 59, No. 1/2, 1998, pp. 53–64.

[43]Beulens, J. J., Milojevic, D., Schram, D. C., and Vallinga, P. M., "A Two-Dimensional Nonequilibrium Model of Cascaded arc Plasma Flows," *Physics of Fluids B*, Vol. 3, No. 9, 1991, pp. 2548–2557.